Self-assembly of hybrid organic-inorganic polyoxovanadates: Functionalised mixed-valent clusters and molecular cages

John M. Breen,[a] Rodolphe Clérac,[b,c] Lei Zhang,[a] Suzanne M. Cloonan,[d,¥] Elaine Kennedy,[d] Martin Feeney,[a] Thomas McCabe,[a] D. Clive Williams,[d] and Wolfgang Schmitt[a]*

SUPPLEMENTARY INFORMATION

Table of Contents

page

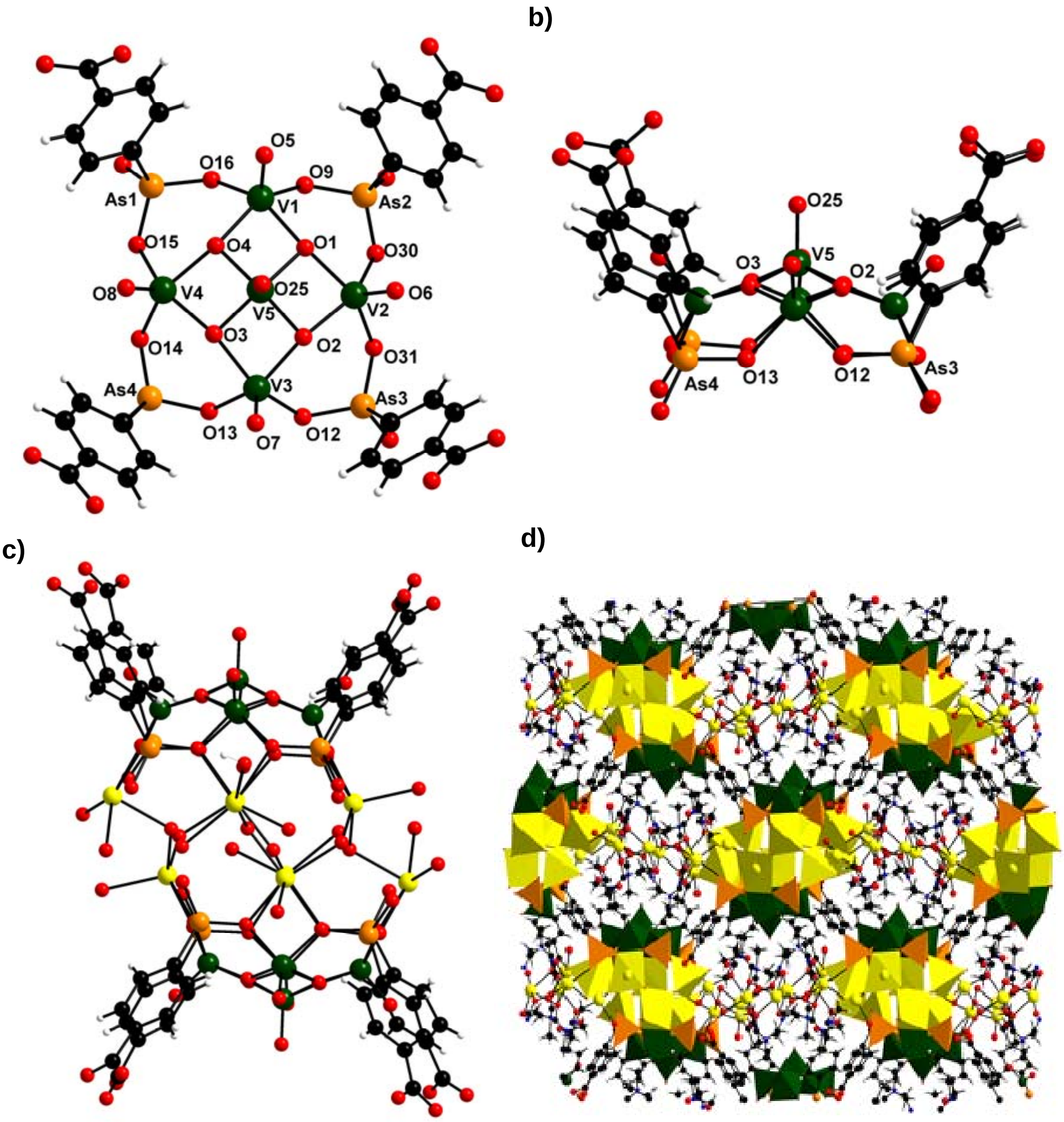

Figure S1: (a) A ball and stick representation of the anionic core $[V_5O_9(O_3AsC_6H_4\text{-}4\text{-}COO)_4]^{9-}$ viewed along the crystallographic *c*-axis. (b) A side on view of the anionic core as viewed along the crystallographic *b*-axis. (c) A ball and stick representation of two anionic clusters of **2** showing the coordinated sodium counter-ions sandwiched between these two pentanuclear core structures. (d) A polyhedral representation of these cores when viewed in the direction of the crystallographic *a*-axis Colour code: V green, Na yellow, As orange, O red, N blue, C black, H white.

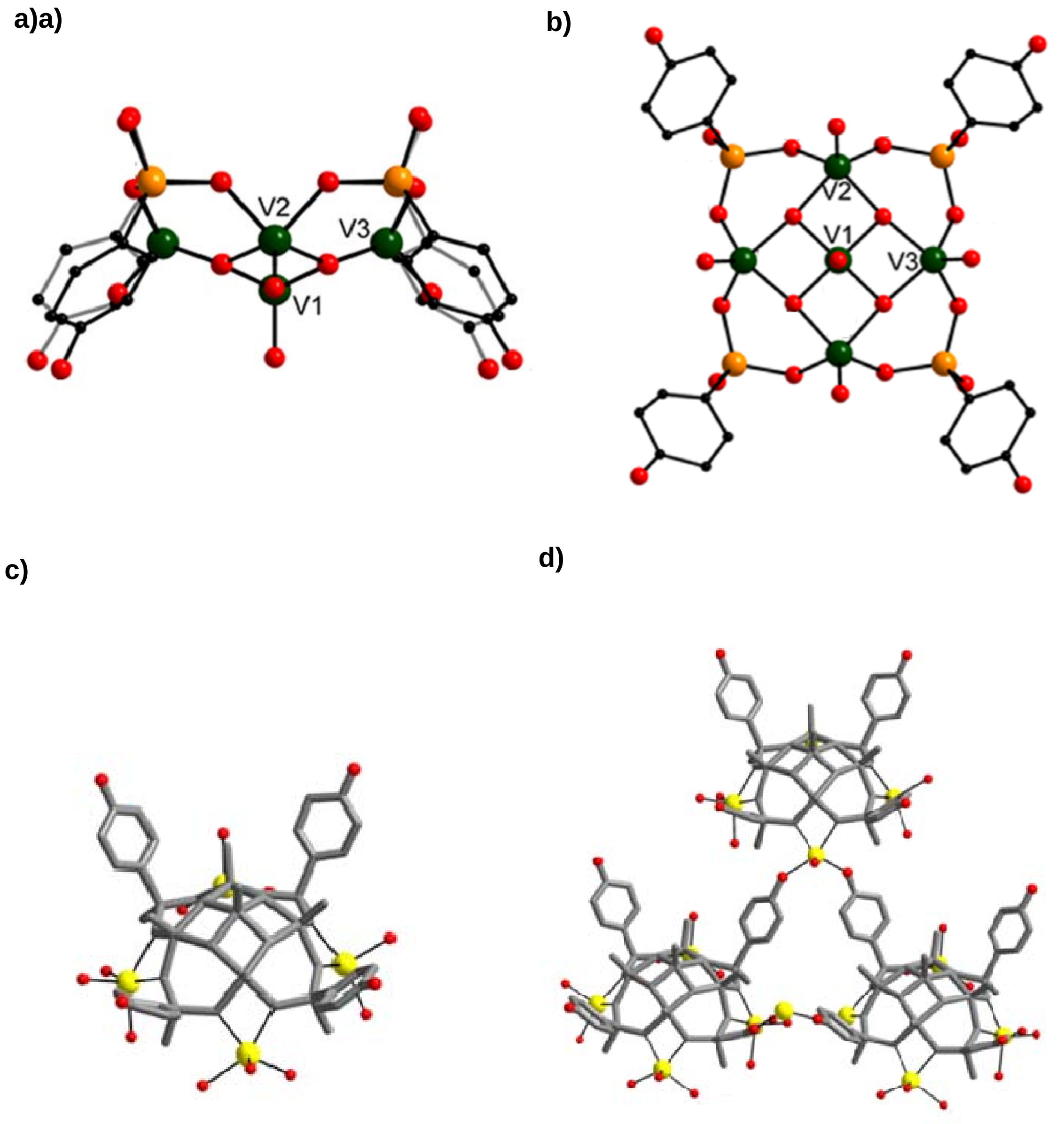

Figure S2: (a) A ball and stick representation of the hybrid polyoxovanadate core of **3** as viewed along the crystallographic *b*-axis. (b) The plan view of the pentanuclear complex as viewed along the crystallographic *c*-axis. (c) A grey wire frame representation of the pentanuclear complex **3**. (d) The nature of the connectivity of the sodium counter-ions between neighbouring pentanuclear units is shown. Disordered water molecules have been omitted for clarity. Colour code: V green, As orange, Na yellow, O red, N blue, C black, H white.

Table S1: Bond Valence Sum calculations for Na_9[**2**]·6DMF·24H_2O

V site	**BVS**	**Assigned O.S**
V(1)	4.048	+4
V(2)	4.001	+4
V(3)	3.966	+4
V(4)	4.056	+4
V(5)	4.826	+5
μ_3-O (1) (2) (3) (4)	2.021 – 2.044	-2
μ-O (9) (12) (13) (14) (15) (16) (30) (31)	2.044 – 2.163	-2
$O_{terminal}$ (5) (6) (7) (8) (25)	1.541 – 1.635	-2

Table S2: Bond Valence Sum calculations for Na_4H[**3**]·5DMF·7H_2O

V site	**BVS**	**Assigned O.S**
V(1)	4.695	+5
V(2)	4.086	+4
V(3)	3.953	+4
μ_3-O (1) (2)	2.823, 2.773	-2
μ-O (6) (7) (10) (11)	1.793 – 1.914	-2
$O_{terminal}$ (8)(9)	1.658, 1.592	-2

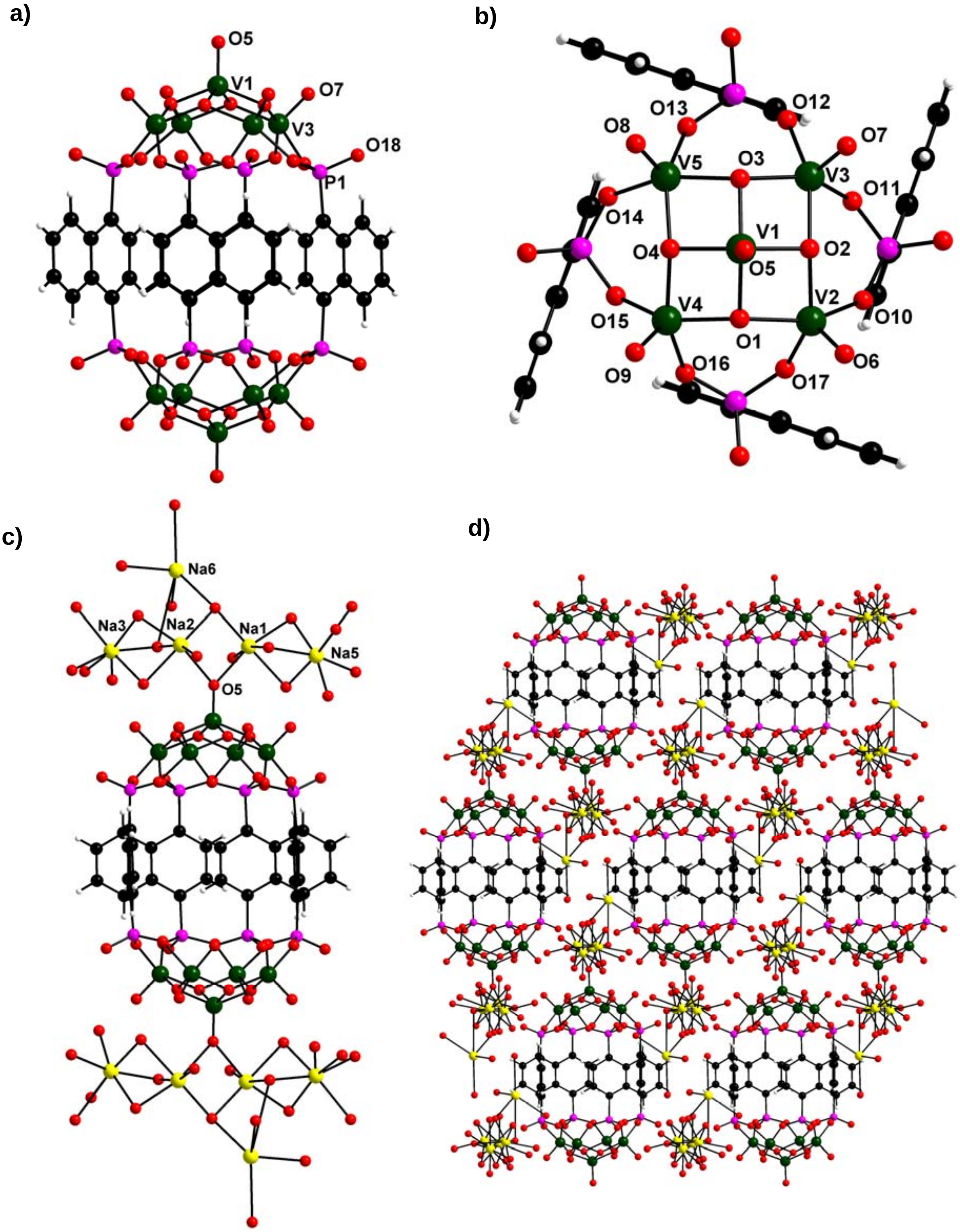

Figure S3: (a) A ball and stick representation of the anionic cluster in Na$_{10}$[**5**]·51.5H$_2$O when viewed along the direction of the crystallographic *b*-axis. (b) A perspective view of the 'edge to face' arrangement of the naphthalene phosphonate ligands. (c) Connectivity of the solvated pentanuclear sodium unit (and symmetry equivalents) to the anionic cluster **5**. (d) The packing arrangement of the sodium counter-ions in crystal structure of Na$_{10}$[**5**]·51.5H$_2$O when viewed along the crystallographic *b*-axis. Disordered solvents molecules and hydrogen atoms have been deleted for clarity. Colour code: V green, Na yellow, P purple, O red, C black.

Table S3: Bond Valence Sum calculations for Na_{10}[**5**]·51.5H_2O

V site	**BVS**	**Assigned O.S**
V(1)	4.545	+5
V(2)	4.079	+4
V(3)	4.128	+4
V(4)	4.119	+4
V(5)	4.053	+4
μ_3-O (1) (2) (3) (4)	1.963 – 1.984	-2
μ-O (10) (11) (12) (13) (14) (15) (16) (17)	1.803 – 1.906	-2
$O_{terminal}$ (5) (6) (7) (8) (9)	1.588 – 1. 955	-2

Thermogravimetric analysis and infrared spectroscopy of Na_9[2]·6DMF·24H_2O, Na_4H[3]·5DMF·7H_2O and Na_{10}[5]·51.5H_2O

The stabilities of the compounds were investigated by thermogravimetric analysis. The measurements were carried out using a Perkin Elmer Pyris TGA under air flow using platinum crucibles (*ca.* 5 mg sample; heating rate of 10 °C min^{-1}; range 25–800 °C). Figures S4 and S5 show the thermogravimetric analyses of Na_9[**2**]·6DMF·24H_2O and Na_4H[**3**]·5DMF·7H_2O, respectively. The decomposition behaviour of Na_9[**2**]·6DMF·24H_2O and Na_4H[**3**]·5DMF·7H_2O is characterised by solvent loss in the temperature regime between *ca.* 25–200 °C. Oxidation of the organic ligands occurs above *ca.* 300 °C.

Figures S6 shows the thermogravimetric analyses of Na_{10}[**5**]·51.5H_2O. The decomposition behaviour of Na_{10}[**5**]·51.5H_2O in air is characterised by the loss of the water molecules between *ca.* 25 and 250 °C. Oxidation of the aromatic bisphosphonate ligands occurs similarly above *ca.* 300 °C.

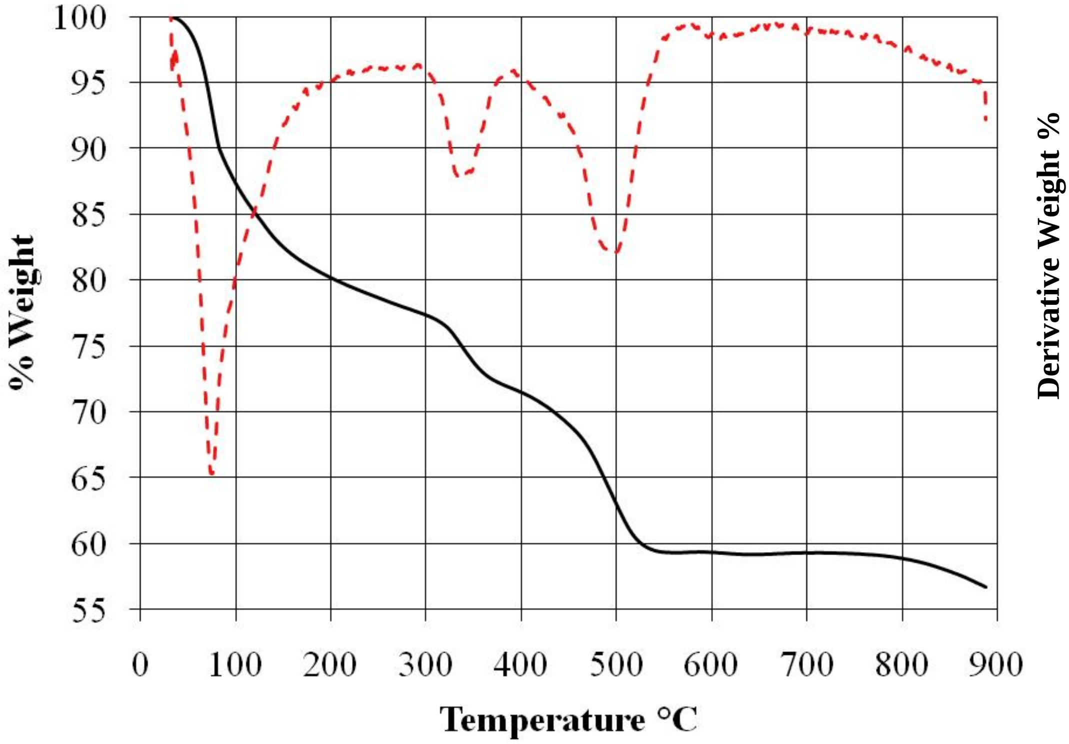

Figure S4. TGA (solid line) and DTA (dotted line) of Na_9[**2**]·6DMF·24H_2O.

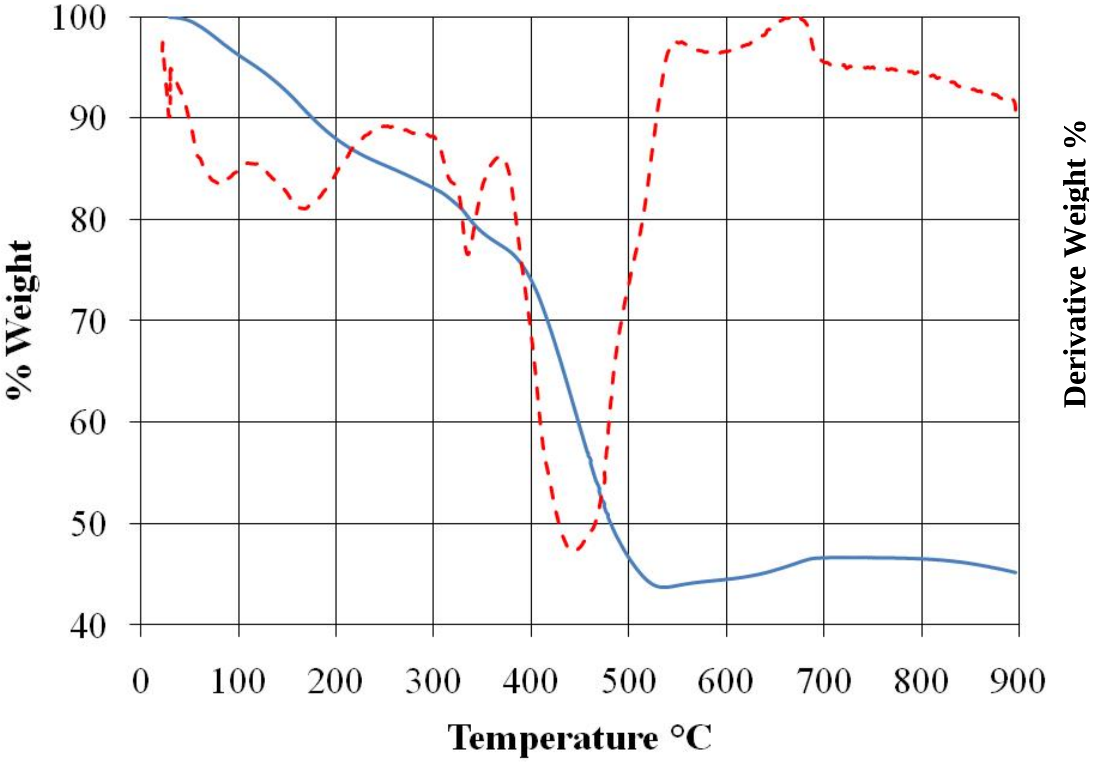

Figure S5. TGA (solid line) and DTA (dotted line) of $Na_4H[\mathbf{3}]\cdot5DMF\cdot7H_2O$.

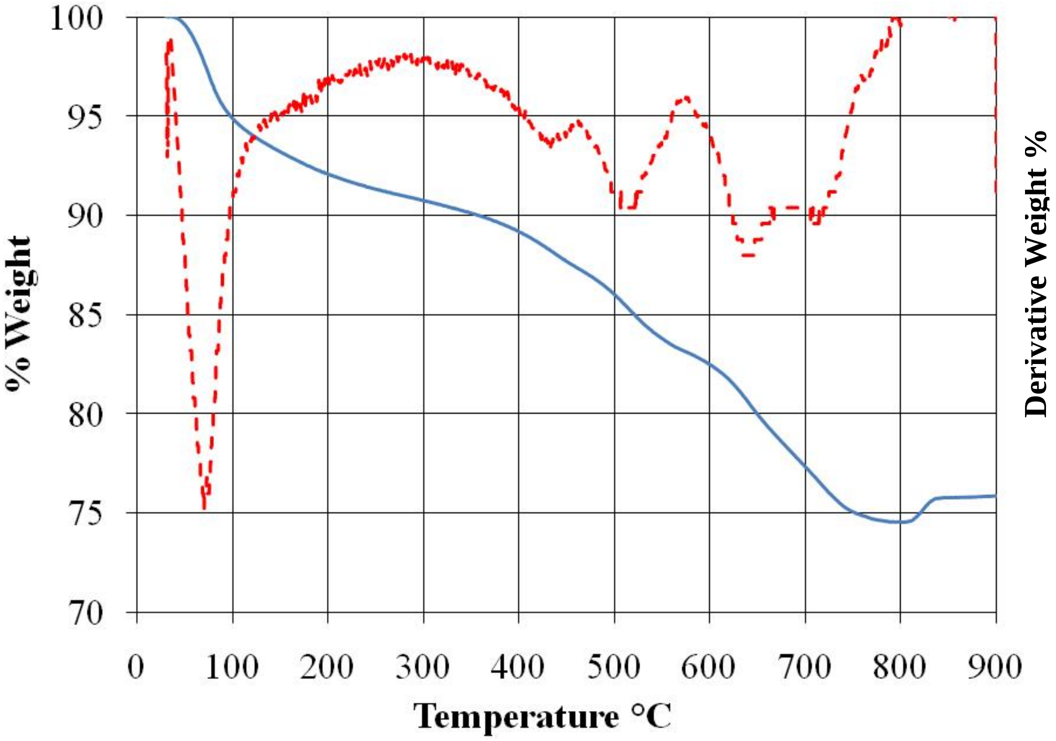

Figure S6. TGA (solid line) and DTA (dotted line) of $Na_{10}[\mathbf{5}]\cdot51.5H_2O$.

UV-VIS spectroscopy of $Na_9[2]·6DMF·24H_2O$, $Na_4H[3]·5DMF·7H_2O$ and N

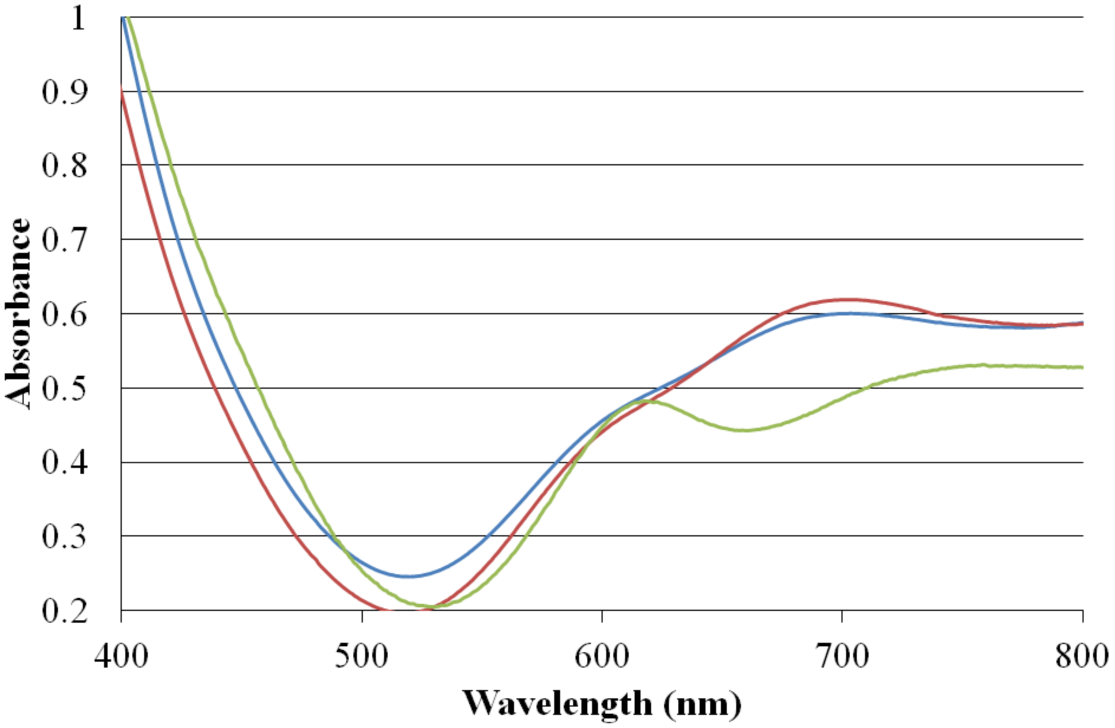

Figure S7. UV-Vis spectrum a 1 mM solution of $Na_9[\mathbf{2}]·6DMF·24H_2O$ (blue) and $Na_4H[\mathbf{3}]·5DMF·7H_2O$ (red) in DMSO. UV-vis spectrum of a 1 mM solution of $Na_{10}[\mathbf{5}]·51.5H_2O$ (green) dissolved in water.

Electrospray Ionisation Mass Spectrometry (ESI-MS)

Electrospray ionization (ESI) mass spectra were collected using a TOF-MS (Time-of-Flight – Mass Spectrometry, LCT Premier) instrument supplied by Waters Corp. with Leucine-Enkephalin (Leu-Enk) as an accurate mass reference. All data, including simulated isotope patterns and molecular weight calculations, were processed using Masslynx version 4.0 (Waters Corp.) data analysis software. Sample was introduced into the MS via a liquid chromatography inlet at 200 μL min^{-1}, whilst a Leu-Enk solution (10 μg mL^{-1} in acetonitrile/ 0.1 TFA in water, 50:50, v/v) was co-injected via a micropump at 2 μL min^{-1}. The ESI settings were set with the nebuliser gas and desolvatation gas at 60 and 500 L h^{-1}, respectively. Source and desolvatation gas temperature were set at 100 and 200 °C, respectively. The ion polarity for all MS scans were recorded in negative mode with voltage of the capillary tip set between 2.5-3 kV, sample cone at 30 V, extraction cone at 3 V, RF value set between 700-1200, m/z range set between 100-2100, scan time at 0.9 sec and inter-scan delay set at 0.1 sec

Table S4. ESI-MS assignment for **1-7**.

Clusters (dissolving solvent)	(m/z)	Species attributed
1 (DMSO)	1262.5	$H_4[V_5O_9(O_3AsC_6H_4NH_2)_4]^-$
2 (DMSO)	Not seen	Not seen
3 (DMSO)	1266.5	$H_4[V_5O_9(O_3AsC_6H_4OH)_4]^-$
4 (DMSO)	1559.4	$Na_3H_3[V_{12}O_{18}(AsO_3C_6H_4NH_2)_{10}]^{2-}$
	1571.4	$Na_4H_2[V_{12}O_{18}(AsO_3C_6H_4NH_2)_{10}]^{2-}$
	1589.4	$Na_4H_2[(H_2O)_2V_{12}O_{18}(AsO_3C_6H_4NH_2)_{10}]^{2-}$
5 (H_2O)	970.6	$H_8[V_{10}O_{18}(O_3PC_{10}H_6PO_3)_4]^{2-}$
	981.6	$NaH_7[V_{10}O_{18}(O_3PC_6H_4PO_3)_4]^{2-}$
	992.6	$Na_2H_6[(V_5O_9)_2(O_3PC_6H_4PO_3)_4]^{2-}$
6 (H_2O)	870.6	$H_8[V_{10}O_{18}(O_3PC_6H_4PO_3)_4]^{2-}$.
	881.6	$NaH_7[V_{10}O_{18}(O_3PC_6H_4PO_3)_4]^{2-}$
	892.6	$Na_2H_6[V_{10}O_{18}(O_3PC_6H_4PO_3)_4]^{2-}$
	574.0	$H_7[V_{10}O_{18}(O_3PC_6H_4PO_3)_4]^{3-}$ $-H_2O$
7 (H_2O)	1022.7	$H_8[(V_5O_9)_2(O_3PC_{12}H_8PO_3)_4]^{2-}$
	1033.7	$NaH_7[(V_5O_9)_2(O_3PC_{12}H_8PO_3)_4]^{2-}$
	1044.7	$Na_2H_6[(V_5O_9)_2(O_3PC_{12}H_8PO_3)_4]^{2-}$
	675.4	$H_7[(V_5O_9)_2(O_3PC_{12}H_8PO_3)_4]^{3-}$ $-H_2O$

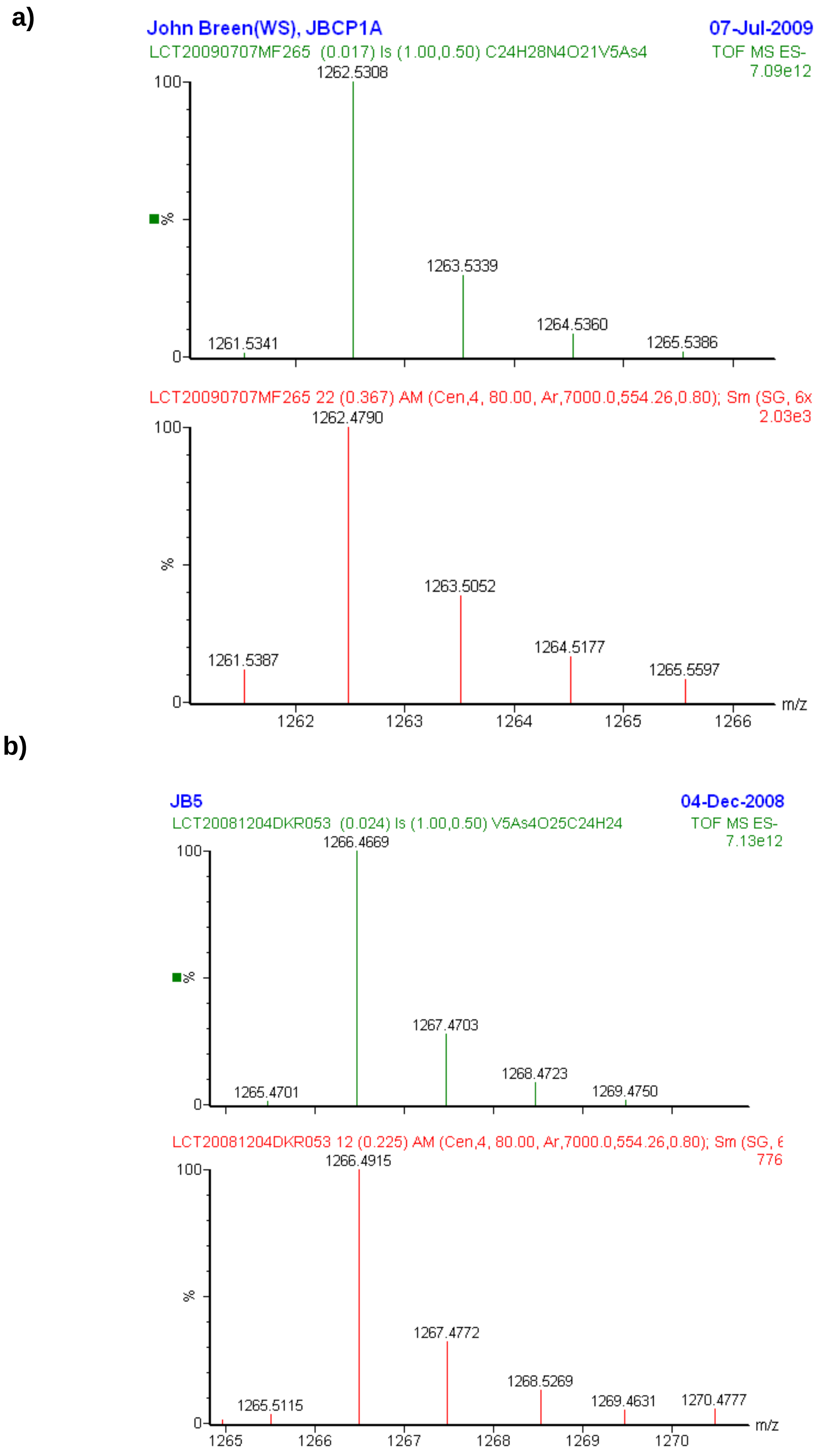

Figure S8: (a) Mass spectra of **1** in DMSO (b) Mass spectra of **3** in DMSO. Experimental spectra in *red*; model spectra in *green;* for assignment see Table S4.

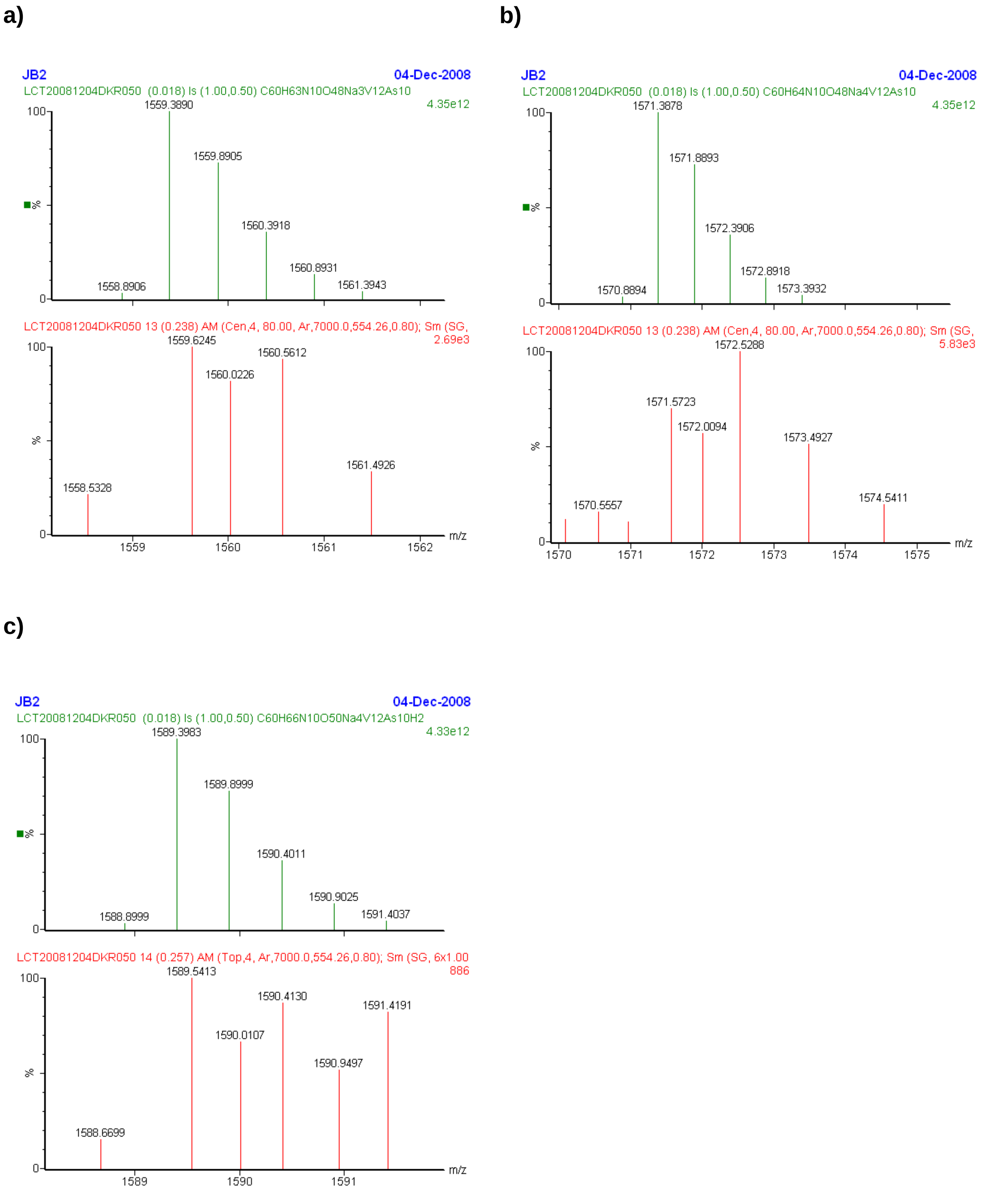

Figure S9: (a-c) Mass spectra of different charged species of **4** in DMSO. Experimental spectra in *red*; model spectra in *green;* for assignment see Table S4.

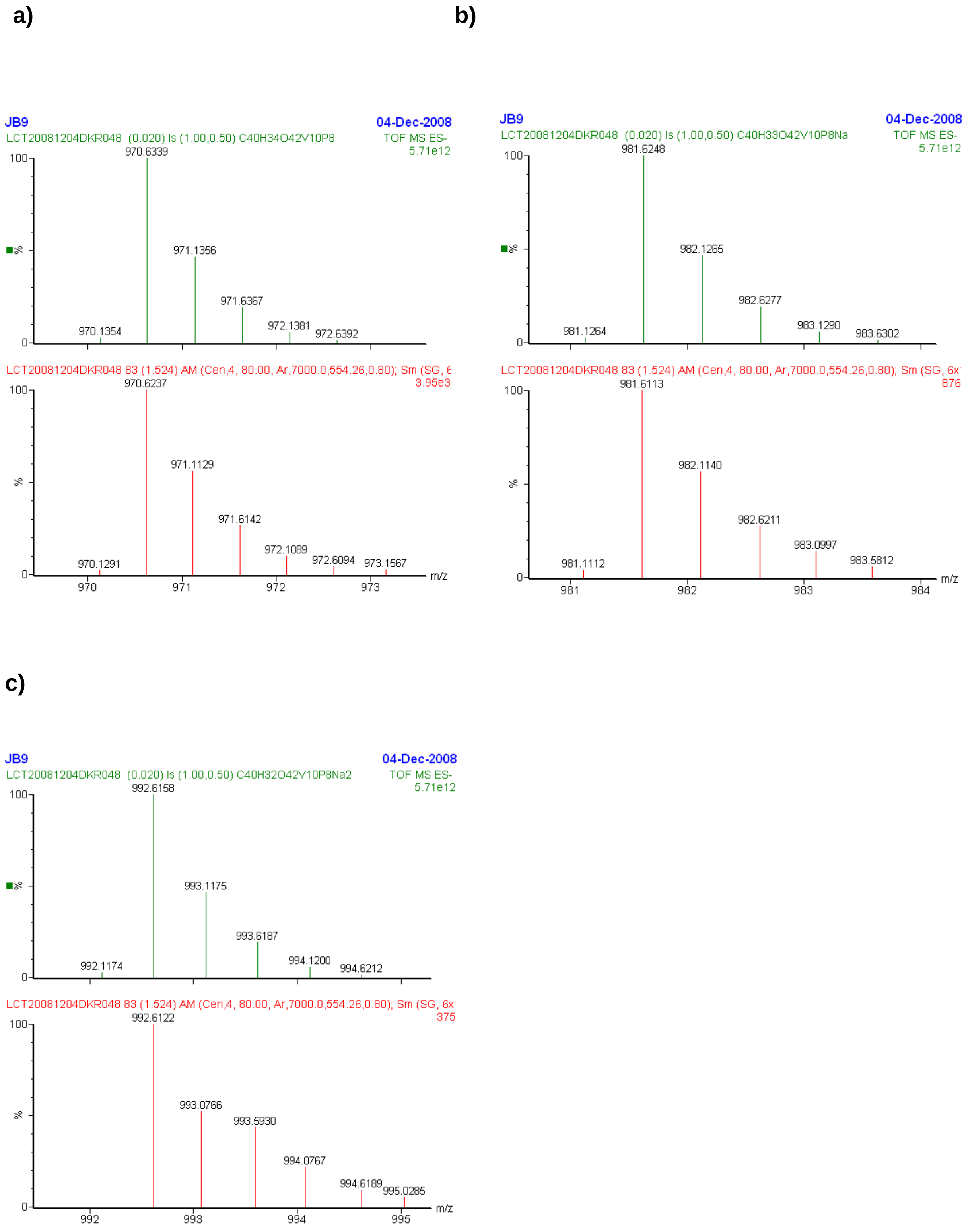

Figure S10: (a-c) Mass spectra of different charged species of **5** in water. Experimental spectra in *red*; model spectra in *green;* for assignment see Table S4.

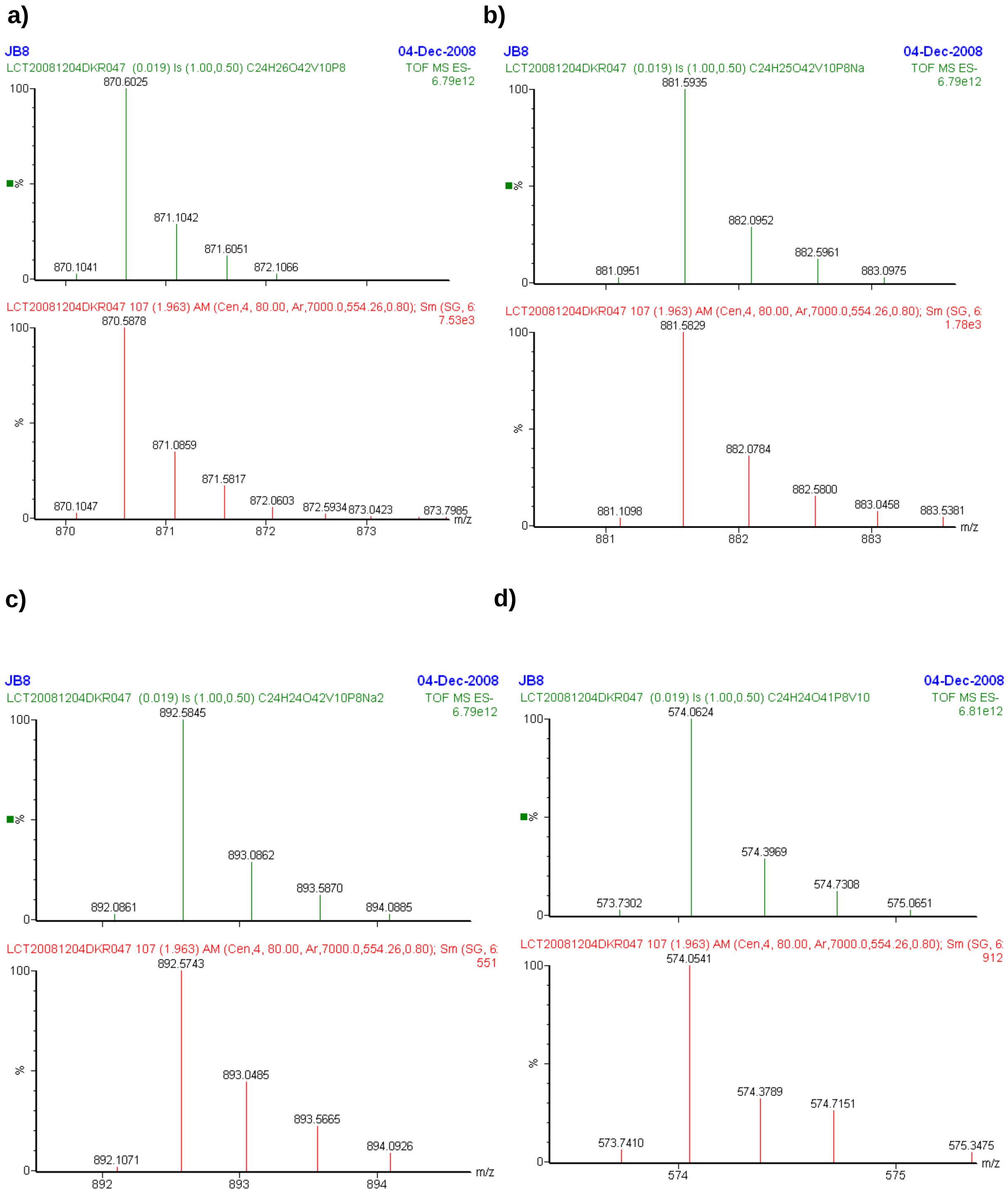

Figure S11: (a-c) Mass spectra of different charged species of **6** in water. Experimental spectra in *red*; model spectra in *green;* for assignment see Table S4.

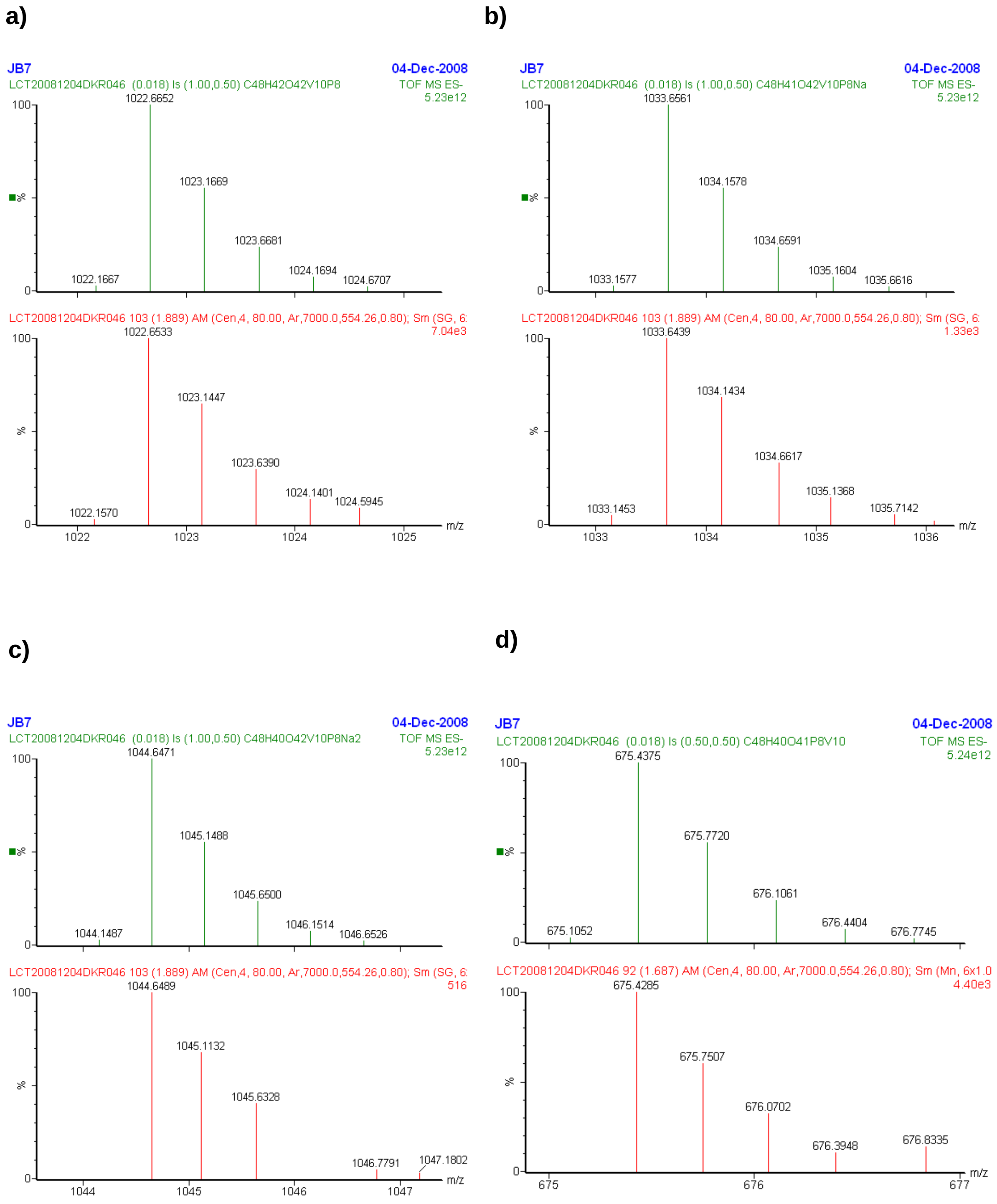

Figure S12: (a-c) Mass spectra of different charged species of **7** in water. Experimental spectra in *red*; model spectra in *green;* for assignment see Table S4.

Cell viability studies of three different cancer cell lines (Mutu-I, A549, K562) with respect to different concentrations of $Na_8[\mathbf{6}]\cdot 32H_2O$ and $Na_8[7]\cdot 2DMF\cdot 29H_2O$.

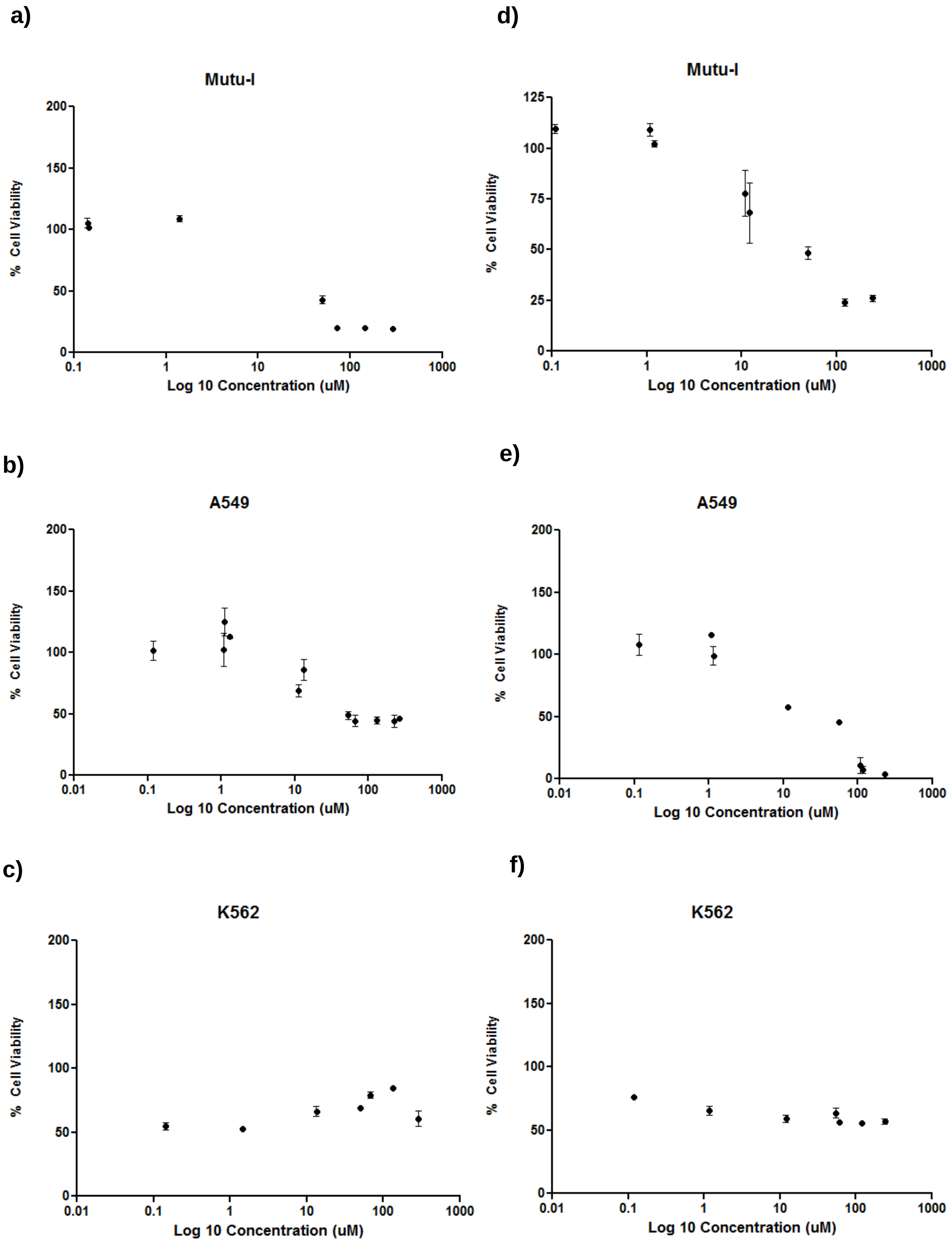

Figure S13: Cell viability studies of the three different cancer lines with respect to different concentrations of $Na_8[\mathbf{6}]\cdot 32H_2O$ (a-c) and $Na_8[\mathbf{7}]\cdot 2DMF\cdot 29H_2O$ (d-f) .

Compound	**EC_{50}**		
	A549	*MUTU-I*	*K562*
Na_8[**6**]·32H_2O	50μM	40μM	-
Na_8[**7**]·2DMF·29H_2O	40μM	50μM	-
Vanadyl Sulfate	150μM	500μM	-
Sodium Orthovanadate	-	-	-
p-arsanilic acid,	-	-	-
1,4-benzenebisphosphonic acid	-	-	-
[1,1'-biphenyl]-4,4'-diylbis-phosphonic acid	-	-	-

Experimental: The A549 cell line was generated through explant culture of lung carcinomatous tissue from a 58-year-old Caucasian male[1] and was cultured in DMEM supplemented with 10% (v/v) FBS and Penicillin and Streptomycin (100μg/ml). The MUTU-I (c179) cell line is an isogenic stable group I Burkitt's lymphoma (BL), cell line derived from a BL biopsy.[2] The K562 cell line was established from the pleural effusion of a 53-year-old female with chronic myelogenous leukemia in terminal blast crises.[3] The above cell lines were cultured in RPMI-1640 medium containing phenol red and supplemented with 10% (v/v) fetal bovine serum (FBS), L-glutamine (2mM), penicillin and streptomycin (100 μg/mL). The MUTU-I c179 cell line required the additional supplements of alpha-thioglycerol (5mM in phosphate buffered saline (PBS) with 20 μM bathocuprione disulphonic acid), sodium pyruvate (100 mM) and HEPES (1 mM).

Alamar Blue Assay for anti-proliferative activity: 1-5 x 10^4 cells/well were seeded in a 96-well plate and treated with the respective drug for 24 hrs. Each well was then treated with 20 μL of Alamar Blue (pre-warmed to 37 ˚C) and left to incubate at 37 ˚C in the dark for 4-6 h. Fluorescence was read using at 590 nm (excitation 544 nm). The background fluorescence of the media without cells + Alamar Blue was taken away from each group, and the control untreated cells represented 100% cell viability. Sodium azide (1mM) was used as a positive control for cell death in each of the cell lines, resulting in 90% cytotoxicity.

1. D. J. Giard, S. A. Aaoronson, G. J. Todaro, P. Arnstein, J. K. Kersey, H. Dosik and W. Parks, *J. Natl. Cancer Inst.*, 1973, **51**, 1417.
2. M. P. Baker, A. G. Eliopoulos, L. S. Young, R. J. Armitage, C. D. Gregory and J. Gordon, *Blood*, 1998, **92**, 2830.
3. C. B. Lozzio and B. B. Lozzio, *Blood*, 1975, **45**, 321.

Magnetic properties of $Na_4[4]\cdot1.5DMF\cdot12.25H_2O$

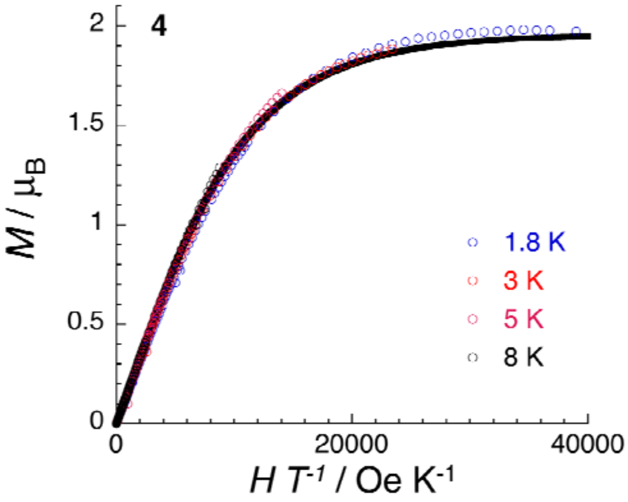

Figure S14: – Field dependence of the magnetization for $Na_4[4]\cdot1.5DMF\cdot12.25H_2O$; Solid lines are the best fit of the experimental data to the $S = 1$ Brillouin function (data per $\{AsV_4O_8\}\{V_2O_2\}$ motif).

.